Supplement of

Impacts of the heterogeneous ammonia uptake on air quality in the North China Plain

Yuxuan Lu et al.

Correspondence to: Ningning Zhang (zhangnn@ieecas.cn)

SI. Model description and configuration

A specific version of the WRF-Chem model is used in this study, modified by Li et al. at the Molina Center for Energy and the Environment (Li et al., 2010; Li et al., 2011a; Li et al., 2011b). This version applies the Community Multi-scale Air Quality (CMAQ) aerosol model for the aerosol simulation, which also includes the processes of coagulation, particle growth by the addition of mass, and new particle formation (Binkowski & Roselle, 2003). Aerosols are modeled in CMAQ using a modal approach based on the assumption that particles can be represented by three log normal size distribution. The SAPARC-99 mechanism (Statewide Air pollution Research Centre, version 1999) is used to simulate gas-phase chemistry. Inorganic aerosols are predicted by a thermodynamic model: the ISORROPIA Version 1.7 (Nenes et al., 1998). A non-traditional SOA module containing volatility basis set (VBS) modeling approach is applied to model the secondary organic aerosol (SOA) as well as glyoxal and methylglyoxal contributions (Li et al., 2011b). The photolysis rates of gas-phase species are calculated by the Fast Tropospheric Ultraviolet and Visible (FTUV) radiation module (Li et al., 2005; Tie et al., 2003). The wet deposition follows the method in the CMAQ model, and surface dry depositions are parameterized according to Wesely (1989). The anthropogenic emission inventory with the base year of 2017 is developed by Li et al. (2017) and Zheng et al. (2018), encompassing industrial, agricultural, residential, transportation, and power plant contributions. The biogenic emissions are calculated online using the Model of Emissions of Gases and Aerosols from Nature (MEGAN) (Guenther et al., 2006).

The simulations cover 1-30 November 2017, with the first 36 h discarded as model spin-up. Four simulations are performed to evaluate the effects of NH_3 uptake by SOA, including a base case without the uptake mechanism and three sensitivity cases considering the reaction with uptake coefficient γ equals to 10^{-3}, 10^{-4} and 10^{-5} respectively. All scenarios use the same anthropogenic emissions, meteorological and chemical initial and boundary conditions, and parameterization schemes in the model. Simulation results from the base case are compared with observations for model validation, while the effects of the uptake mechanism are quantified by differentiating base case with sensitivity cases.

S2. Measurements

In this study, model performances are validated using the hourly data of four criteria species ($PM_{2.5}$, O_3, NO_2, SO_2) downloaded from http://www.aqistudy.cn/. The daily aerosol components, including organic carbon (OC), elemental carbon (EC), sulfate, nitrate, and ammonium are from filter measurement in the cities in North China Plain and surrounding areas. The NH_3 mass concentrations at Xianghe station are collected using a

diffusive sampler (Analysts, CNR-Institute of Atmospheric Pollution, Roma, Italy) (Pan et al., 2018). NOCs component data is obtained from large flow filter measurement at Xianghe station. Seven chemical classes of NOCs are determined in filter measured $PM_{2.5}$ samples, including free amino acids, amines, amides, nitriles, isocyanates, urea, and cyclic NOCs (Wang, et al., 2022). The total column NH_3 products from the Infrared Atmospheric Sounding Interferometer (IASI) onboard the Metop-B and Metop-C satellites are used to evaluate the simulated spatial distribution of NH_3 over the NCP. The NH_3 products used in this study are retrieved using the neural network-based algorithm developed by Whitburn et al. (2016) and Van Damme et al. (2017), which has been extensively validated against independent datasets. To ensure high data quality, only daytime IASI columns are considered, as night time measurements tend to have larger relative errors due to the generally low thermal contrast (Van Damme et al., 2014). Furthermore, only data with relative uncertainties lower than 40% are retained for the comparison.

We use the OC/EC ratio approach evaluate the OA concentration from the filter measured OC and EC concentrations (Strader, 1999; Cao et al., 2003; 2004). The following method is used to derive the "measured" POA, SOA, and OA mass concentrations from EC and OC filter measurements:

$$POC = EC \times (POC/EC\ ratio)$$

$$SOC = OC - POC$$

$$POA = POC \times (POA/POC\ ratio)$$

$$SOA = SOC \times (SOA/SOC\ ratio)$$

$$OA = POA + SOA$$

Numerous studies have been performed to investigate the POA/POC and SOA/SOC ratios (Aiken et al., 2008; Yu, 2011; Yu et al., 2009), which can be used to obtain OA concentrations from measured EC and OC concentrations. In this study, the POC/EC, POA/POC, SOA/SOC ratios are assumed to be 2.4, 1.2, and 1.6, respectively, based on the previous studies (Cao et al., 2007; Aiken et al., 2008; Yu, 2011; Yu et al., 2009). It is worth to note that, these assumed values might affect the model-measurement comparisons.

Using the measured EC and OC concentrations, the SOA/EC ratio is calculated:

$$(SOA/EC\ ratio) = (SOA/SOC\ ratio) \times (SOC/EC\ ratio)$$

$$= (SOA/SOC\ ratio) \times [(OC - POC) / EC]$$

$$= (SOA/SOC\ ratio) \times [(OC/EC\ ratio) - (POC/EC\ ratio)]$$

And the POA/EC ratio is derived following:

$$(POA/EC\ ratio) = (POA/POC\ ratio) \times (POC/EC\ ratio)$$

S3. Statistical methods for model evaluation

Four statistical methods are employed to evaluate the model performance on simulating gas-phase species along with aerosol components against measurements, including the mean bias (MB), root mean square error (RMSE), the index of agreement (IOA) and the correlation coefficient (R).

$$MB = \frac{1}{N}\sum_{i=1}^{N}(P_i - O_i)$$

$$RMSE = \left[\frac{1}{N}\sum_{i=1}^{N}(P_i - O_i)^2\right]^{\frac{1}{2}}$$

$$IOA = 1 - \frac{\sum_{i=1}^{N}(P_i - O_i)^2}{\sum_{i=1}^{N}(|P_i - \overline{O}| + |O_i - \overline{O}|)^2}$$

$$R = \frac{\sum_{i=1}^{N}[(\overline{P} - P_i) \times (O_i - \overline{O})]}{\sum_{i=1}^{N}(P_i - \overline{P})^2 \times \sum_{i=1}^{N}(O_i - \overline{O})^2}$$

Where P_i and O_i denote the concentration of predicted and observed concentration. N is the total number of predictions used for comparison, $\overline{O}$ and $\overline{P}$ are the average concentration of observation and prediction. IOA indicates the relative difference between the predicted value and the measured value with a range of 0-1. The closer IOA is to 1, the better the model performances. The R ranges from −1 to 1, with 1 implying perfect spatial consistency of observation and prediction.

S4. Model validation

Figure S1 presents the diurnal profiles of observed and simulated near-surface $PM_{2.5}$, O_3, NO_2, and SO_2 concentrations averaged across monitoring sites in the NCP from 31 October to 31 November 2017. The model well captures the temporal variations of $PM_{2.5}$ concentrations in the NCP against observations, with an IOA of 0.93. While it slightly overestimates $PM_{2.5}$ levels compared to measurements, the MB is 0.6 μg m^{-3}. The model successfully reproduces key diurnal features of O_3, including afternoon peaks driven by active photochemical reactions and low nighttime levels due to NOx titration, with an IOA of 0.84. However, the model tends to underestimate the O_3 concentration compared to measurements, especially during the first few days of simulation period, causing an overall MB of -1.5 μg m^{-3}. NO_2 simulations are also reasonably consistent with observations, with an IOA of 0.83 and MB of -1.9 μg m^{-3}, though notable deviations (both overestimates and underestimates) persist in certain periods. The model reasonably well captures the temporal variation of SO_2 concentrations against observations, with an IOA of 0.67. SO_2 simulations exhibit greater uncertainties, partly because SO_2 is mainly emitted from point sources, and is therefore more sensitive to wind field uncertainties

(Bei et al., 2017).

Figure S2 shows the simulated and observed spatial distributions of mean mass concentrations of $PM_{2.5}$, O_3, NO_2, and SO_2 during the simulation episode. The model successfully captures the prominent $PM_{2.5}$ hotspots in southern Hebei, western Shandong, and northern Henan, where monthly mean concentrations frequently exceeded 90 $\mu g\ m^{-3}$ due to the synergy of intense local emissions and stagnant meteorological conditions. The spatial distributions of O_3, NO_2, and SO_2 are also satisfactorily reproduced, demonstrating that the simulated spatial patterns are in robust agreement with observations from ambient monitoring stations.

SI References

Aiken, A. C., DeCarlo, P. F., Kroll, J. H., Worsnop, D. R., Huffman, J. A., Docherty, K. S., Ulbrich, I. M., Mohr, C., Kimmel, J. R., Sueper, D., Sun, Y., Zhang, Q., Trimborn, A., Northway, M., Ziemann, P. J., Canagaratna, M. R., Onasch, T. B., Alfarra, M. R., Prévôt, A. S. H., Dommen, J., Duplissy, J., Metzger, A., Baltensperger, U. and Jimenez, J. L.: O/C and OM/OC Ratios of Primary, Secondary, and Ambient Organic Aerosols with High-Resolution Time-of-Flight Aerosol Mass Spectrometry, Environ. Sci. Technol., 42(12), 4478–4485, doi:10.1021/es703009q, 2008.

Bei, N., Wu, J., Feng, T., Bei, R., Zhao, S., Cao, J., Tie, X., and Li, G.: Impacts of Meteorological Uncertainties on the Haze Formation in Beijing-Tianjin-Hebei (BTH) during Wintertime: A case study, Atmos. Chem. Phys., 17, 11679–11691, https://doi.org/10.5194/acp-17-11679-2017, 2017.

Binkowski, F. S. and Roselle, S. J.: Models-3 Community Multiscale Air Quality (CMAQ) model aerosol component 1. Model description, J. Geophys. Res. Atmos., 108, 4183, https://doi.org/10.1029/2001JD001409, 2003.

Cao, J. J., Lee, S. C., Ho, K. F., Zhang, X. Y. and Zou, S. C.: Characteristics of carbonaceous aerosol in Pearl River Delta Region, China during 2001 winter period, Atmos. Environ., 37(11), 1451–1460, doi:10.1016/s1352-2310(02)01002-6, 2003.

Cao, J. J., Lee, S. C., Ho, K. F., Zou, S. C., Fung, K., Li, Y., Watson, J. G. and Chow, J. C.: Spatial and seasonal variations of atmospheric organic carbon and elemental carbon in Pearl River Delta Region, China, Atmos. Environ., 38(27), 4447–4456, doi:10.1016/j.atmosenv.2004.05.016, 2004.

Cao, J. J., Zhu, C. S., Tie, X. X., Geng, F. H., Xu, H. M., Ho, S. S. H., Wang, G. H., Han, Y. M. and Ho, K. F.: Characteristics and sources of carbonaceous aerosols from Shanghai, China, Atmos. Chem. Phys., 13(2), 803–817, doi:10.5194/acp-13-803-2013, 2013.

DeCarlo, P. F., Kimmel, J. R., Trimborn, A., et al.: Field-Deployable, High-Resolution, Time-of-Flight Aerosol Mass Spectrometer, Anal. Chem., 78, 8281–8289, https://doi.org/10.1021/ac061249n, 2006.

Guenther, A., Karl, T., Harley, P., Wiedinmyer, C., Palmer, P. I., and Geron, C.: Estimates of global terrestrial isoprene emissions using MEGAN (Model of Emissions of Gases and Aerosols from Nature), Atmos. Chem. Phys., 6, 3181–3210, https://doi.org/10.5194/acp-6-3181-2006, 2006.

Li, G., Zhang, R., Fan, J., and Tie, X.: Impacts of black carbon aerosol on photolysis and ozone, J. Geophys. Res.-Atmos., 110, D23206, https://doi.org/10.1029/2005JD005823, 2005.

Li, G., Lei, W., Zavala, M., Volkamer, R., and Molina, L. T.: Impacts of HONO sources on the photochemistry in Mexico City during the MCMA-2006/MILAGO Campaign, Atmos. Chem. Phys., 10, 6551–6567, https://doi.org/10.5194/acp-10-6551-2010, 2010.

Li, G., Bei, N., Tie, X., and Molina, L. T.: Aerosol effects on the photochemistry in Mexico City during MCMA-2006/MILAGRO campaign, Atmos. Chem. Phys., 11, 5169–5182, https://doi.org/10.5194/acp-11-5169-2011, 2011a.

Li, G., Zavala, M., Lei, W., Tsimpidi, A. P., Karydis, V. A., Pandis, S. N., Canagaratna, M. R., and Molina, L. T.: Simulations of organic aerosol concentrations in Mexico City using the WRF-CHEM model during the MCMA-2006/MILAGRO campaign, Atmos. Chem. Phys., 11, 3789–3809, https://doi.org/10.5194/acp-11-3789-2011, 2011b.

Li, M., Liu, H., Geng, G., Hong, C., Liu, F., Song, Y., Zheng, Y., Yang, X., Yao, Z., Leung, L. R., Zhang, Q., and He, K.: Anthropogenic emission inventories in China: a review, Natl. Sci. Rev., 4, 834–866, https://doi.org/10.1093/nsr/nwx150, 2017.

Nenes, A., Pandis, S. N., and Pilinis, C.: ISORROPIA: A New Thermodynamic Equilibrium Model for Multiphase Multicomponent Inorganic Aerosols, Aquat. Geochem., 4, 123–152, https://doi.org/10.1023/A:1009604003981, 1998.

Pan, Y., Tian, S., Zhao, Y.,Zhang, L., Zhu, B., Gao, J., Huang, J., Chang, Y., Zhu, Y., He, H., Zhang, H., Zhang, L., Wu, Q., Zheng, H., Song, K., Zhou, F., Tian, B., Pan, Z., Huang, S., Wu, J., Liu, Y., Xu, W., Cheng, L., Liu, X., and Wang, Z.: Identifying Ammonia Hotspots in China Using a National Observation Network, Environ. Sci. Technol., 52, 3926–3934, https://doi.org/10.1021/acs.est.7b05235, 2018.

Strader, R., Lurmann, F. W., and Pandis, S. N.: Evaluation of secondary organic aerosol formation in winter, Atmos. Environ., 33(29), 4849–4863, doi:10.1016/s1352-2310(99)00310-6, 1999.

Tie, X., Madronich, S., Walters, S., Edwards, D. P., Ginoux, P., Rasch, P., Zhang, R., and Brasseur, G.: Effect of clouds on photolysis and oxidants in the troposphere, J. Geophys. Res. Atmos., 108, 4642, https://doi.org/10.1029/2003JD003659, 2003.

Van Damme, M., Clarisse, L., Heald, C. L., Hurtmans, D., Ngadi, Y., Clerbaux, C., Dolman, A. J., Erisman, J. W., and Coheur, P. F.: Global distributions, time series and error characterization of atmospheric ammonia NH_3 from IASI satellite observations, Atmos. Chem. Phys., 14, 2905–2922, https://doi.org/10.5194/acp-14-2905-2014, 2014.

Van Damme, M., Whitburn, S., Clarisse, L., Clerbaux, C., Hurtmans, D., and Coheur, P.-F.: Version 2 of the IASI NH_3 neural network retrieval algorithm: near-real-time and reanalysed datasets, Atmos. Meas. Tech., 10, 4905–4914, https://doi.org/10.5194/amt-10-4905-2017, 2017.

Wang, M., Wang, Q., Ho, S. S. H., Li, H., Zhang, R., Ran, W., Qu, L., Lee, S. C., and Cao, J.: Chemical characteristics and sources of nitrogen-containing organic compounds at a regional site in the North China Plain during the transition period of autumn and winter, Sci. Total Environ., 812, 151451, https://doi.org/10.1016/j.scitotenv.2021.151451, 2022.

Wesely, M. L.: Parameterization of surface resistances to gaseous dry deposition in regional-scale numerical models, Atmos. Environ., 23, 1293–1304, https://doi.org/10.1016/0004-6981(89)90153-4, 1989.

Whitburn, S., Van Damme, M., Clarisse, L., Bauduin, S., Heald, C. L., Hadji-Lazaro, J., Clerbaux, C., and Coheur, P.-F.: A flexible and robust neural network IASI-NH_3 retrieval algorithm, J. Geophys. Res.-Atmos., 121, 6581–6599, https://doi.org/10.1002/2016JD024828, 2016.

Yu, X.-Y.: Measurements of carbonaceous aerosols using semi-continuous thermal-optical method, in: Aerosols - Science and Technology, edited by: Guziev, I. A., InTech, Rijeka, Croatia, 461–486, https://doi.org/10.5772/23604, 2011.

Yu, X. Y., Cary, R. A. and Laulainen, N. S.: Primary and secondary organic carbon downwind of Mexico City, Atmos. Chem. Phys., 9(18), 6793–6814, doi:10.5194/acp-9-6793-2009, 2009.

Zheng, B., Tong, D., Li, M., Liu, F., Hong, C., Geng, G., Li, H., Li, X., Peng, L., Qi, J., Yan, L., Zhang, Q., and He, K.: Trends in China's anthropogenic emissions since 2010 as the consequence of clean air actions, Atmos. Chem. Phys., 18, 14095–14111, https://doi.org/10.5194/acp-18-14095-2018, 2018.

Table S1: Model configuration

Region	**The North China Plain**
Simulation period	1 to 30 November 2017
Domain size	300 × 300
Domain center	38°N, 116°E
Horizontal resolution	6 km × 6 km
Vertical resolution	35 vertical levels with a stretched vertical grid with spacing ranging from 30 m near the surface, to 500 m at 2.5 km and 1 km above 14 km
Microphysics scheme	WSM 6-class graupel scheme (Hong and Lim, 2006)
Cumulus scheme	Grell-Devenyi ensemble scheme (Grell and Devenyi, 2002)
Boundary layer scheme	MYJ TKE scheme (Janjić, 2002)
Surface layer scheme	MYJ surface scheme (Janjić, 2002)
Land-surface scheme	Unified Noah land-surface model (Chen and Dudhia, 2001)
Longwave radiation scheme	Goddard longwave scheme (Chou et al., 2001)
Shortwave radiation scheme	Goddard shortwave scheme (Chou and Suarez, 1999)
Meteorological boundary and initial conditions	NCEP 1°×1° reanalysis data
Chemical initial and boundary conditions	MOZART 6-hour output (Horowitz et al., 2003)
Anthropogenic emission inventory	MEIC with the base year of 2017, SAPRC-99 chemical mechanism (Li et al., 2017c; Zheng et al., 2018).
Biogenic emission inventory	Online MEGAN model developed by Guenther et al. (Guenther et al., 2006)

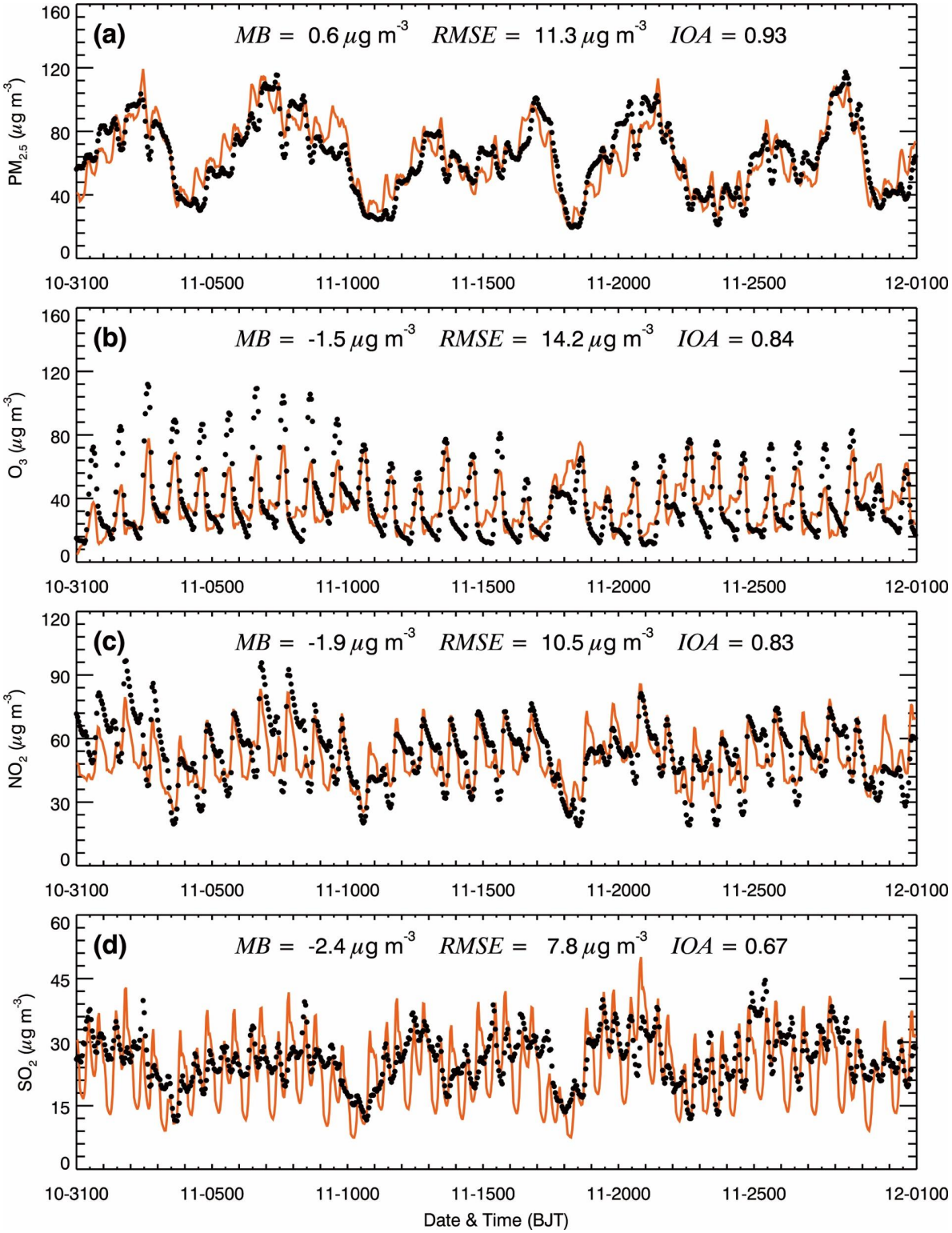

Figure S1: Diurnal profiles of observed (black dots) and simulated (solid red lines) near-surface hourly mass concentrations of (a) $PM_{2.5}$, (b) O_3, (c) NO_2, and (d) SO_2 averaged over all monitoring sites in the NCP in November 2017.

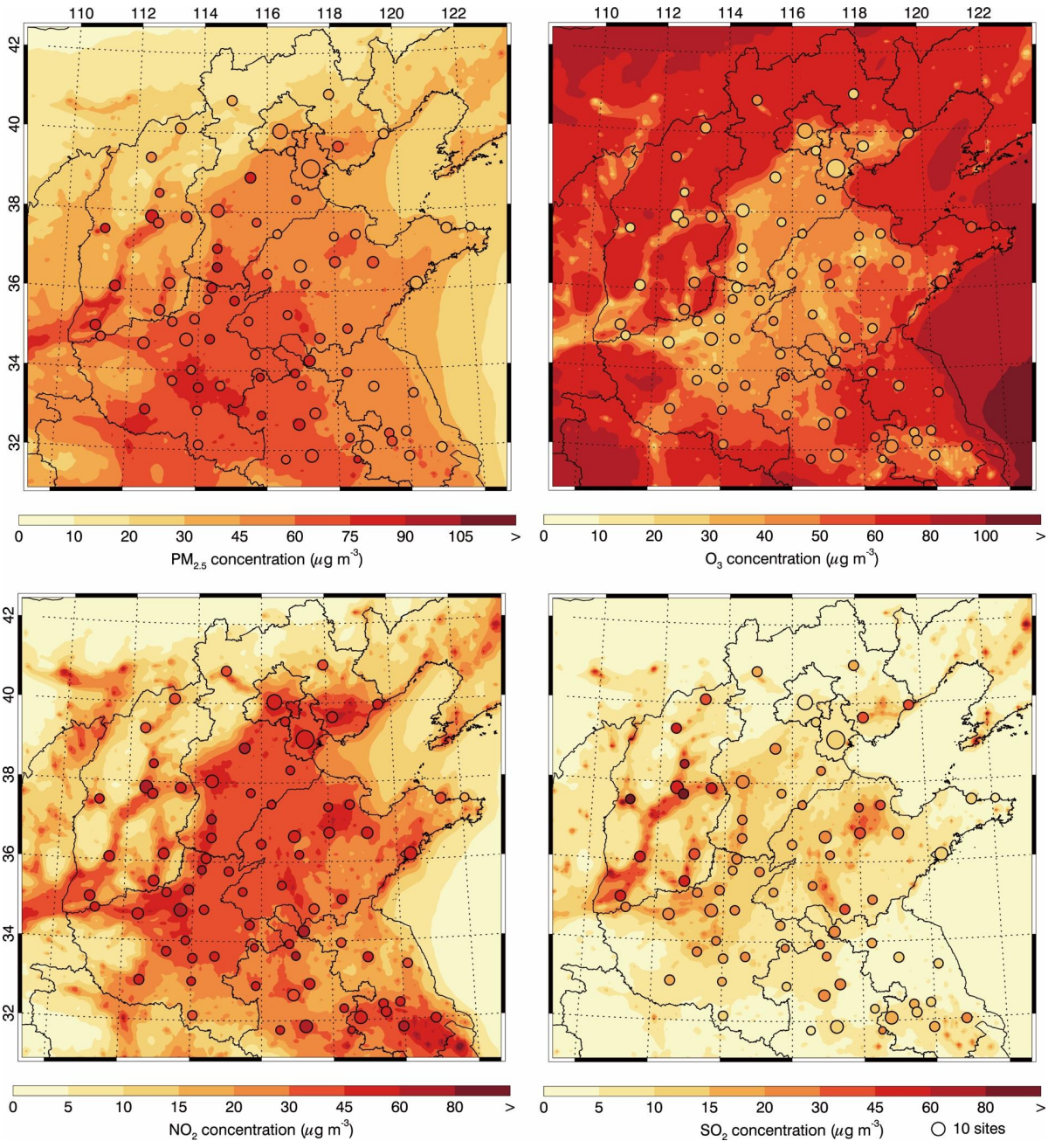

Figure S2: Pattern comparisons of simulated (color contours) versus observed (colored circles) near-surface mass concentrations of (a) $PM_{2.5}$, (b) O_3, (c) NO_2, and (d) SO_2 averaged in November 2017.